ACS APPLIED MATERIALS & INTERFACES

Research Article

www.acsami.org

Variations of Polymer Porous Surface Structures via the Time-Sequenced Dosing of Mixed Solvents

Erik Wrzecionko,[†,‡] Antonín Minařík,*[,†,‡] Petr Smolka,[†,‡] Martin Minařík,[†,‡] Petr Humpolíček,[‡] Petra Rejmontová,[‡] Aleš Mráček,[†,‡] Magda Minaříková,[†,‡] and Lenka Gřundělová[‡]

[†]Department of Physics and Materials Engineering, Tomas Bata University in Zlín, Vavrečkova 275, 760 01 Zlín, Czech Republic
[‡]Centre of Polymer Systems, Tomas Bata University in Zlín, Třída Tomáše Bati 5678, 76001 Zlín, Czech Republic

ABSTRACT: A new approach to polystyrene surface treatment via the time-sequenced dispensing of good and poor solvent mixtures on the rotating surface of treated substrate is presented in this study. It is demonstrated that the variation of the sequencing together with other variables (e.g., temperature and solvent concentration) affects the size and depth of pores evolving on the polystyrene surface. A model of the surface pore creation, associated with the viscoelastic phase separation, surface tension, and secondary flows caused by temperature variations and the rapid evaporation of the good solvent is proposed. Experimental results of profilometric, goniometric, and optical measurements show that this approach enables the simple and quick preparation of surfaces with various numbers, diameters, and depths of individual pores, which ultimately affects not only the wetting characteristics of the surfaces but also the fate of cells cultivated there. The presented method allows the easy preparation of a large number of structured substrates for effective cell cultivation and proliferation.

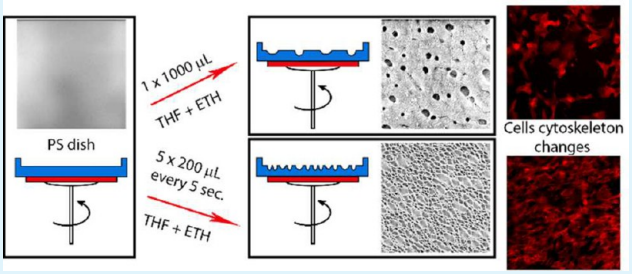

KEYWORDS: *surface, polystyrene, pores, solvent mixture, surface tension, phase separation, wetting, cells*

INTRODUCTION

The self-organized modification of the surface microstructure of polymer materials belongs among the most important postmanufacturing processes, especially for its relative simplicity, rapidity, and uniformity over large areas. The targeted preparation of surface pores has been studied from various points of view due to its wide range of possible applications.[1,2] Such modified materials, characterized by a large specific surface area, are used in many biological, optical, and electrical applications.[3−5] They serve as scaffolds,[6] sites for capturing cells,[7−9] micro reactors,[10−12] self-cleaning surfaces,[13−15] or antireflective layers.[16]

There are many approaches to the surface modification of polymeric materials such as the sol−gel method,[17] plasma etching,[18] mechanical-chemical polishing,[19] and phase separation.[2,20−22]

In this study, a new approach based on the method of the time-sequenced dispensing of a mixture of good and poor solvents on the rotating polystyrene (PS) surface of a treated material is discussed. This process can be seen as a phase separation, which can generally be divided into wet casting and dry casting.[23−26] The phase separation[27] may be caused by different mechanisms: temperature change, poor solvent,[7,28] chemical reaction,[29] or shear deformation.[30] In this study, we induced phase separation by casting a poor solvent, which is separated at the surface and allows the formation of the material by the breath figures approach.[1,2,31,32] The viscoelastic phase separation must also be taken into account in polymer systems, as defined by Tanaka,[33] where the surface tension and resulting Laplace pressure of the poor solvent droplets,[34] interfacial tension,[35] flows induced by rapid solvent evaporation, and temperature gradients[36−42] play significant roles. The interdependent action of these factors is investigated in this work.

The total volume, ratio of the individual components, and the temperature of the solvent mixture are studied in relation to the time sequencing of dosing the mixture of solvents on the polymer surface. We show how these parameters determine the number and size of the generated micropores, thereby consequently changing not only the wettability of the surface but also the viability and cytoskeleton organization of the adhered cells. This brings new insight into the problem of cell interaction with polystyrene-based microstructured surfaces.[7,8,18,43−45]

EXPERIMENTAL SECTION

Materials. Two sizes of PS Petri dishes were used as substrates. Large dishes with a diameter of 5.4 cm, nonsterile (Gosselin), and small dishes with a diameter of 3.4 cm, sterilized by radiation, free from pyrogens and DNA/RNA for cell cultivation (TPP Techno Plastic Products AG), were used. Prior to use, the large unsterilized PS plates were rinsed with alcohol and ultrapure water (18.2 MΩ.cm) followed by drying in an oven at 323 K. Tetrahydrofuran (THF, HPLC grade) and 2-ethoxyethanol p.a. (ETH), both produced by

Received: December 8, 2016
Accepted: January 20, 2017
Published: January 20, 2017

DOI: 10.1021/acsami.6b15774
ACS Appl. Mater. Interfaces 2017, 9, 6472−6481

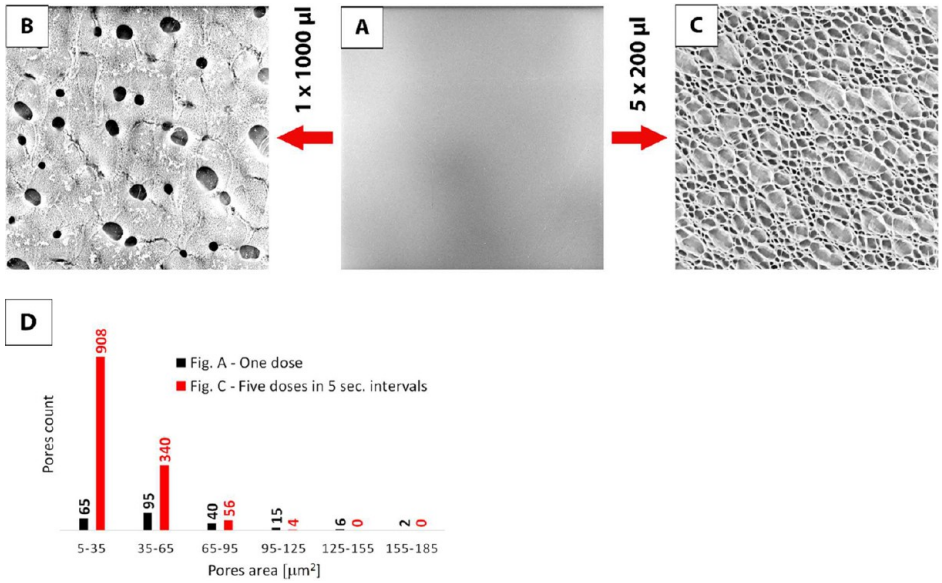

Figure 1. Changes in PS surface appearance due to the division of the solvent mixture volume into smaller doses. (A) Original PS surface, (B) PS surface modified with one dose of the solvent mixtures, and (C) PS surface modified with five doses of the solvent mixtures deposited in five-second intervals. A solvent mixture, THF:ETH, in a volume ratio of 1.5:8.5 at 295 K was used. The SEM images have dimensions of 134 × 134 μm. Pore area distribution in the square 268 × 268 μm is displayed in panel D.

Sigma-Aldrich Ltd., were used for the surface treatment of the PS substrates.

Surface Modification by Spin-Coating. The solvent mixture was deposited on the surface of PS dishes with a homemade spin-coater rotating at 2200 rpm. Dosing of solvents was carried out using a micropipette placed 30 mm above the center of the rotating substrate. Each time, 1−2 mL of a mixed solvent, divided into 1−10 consecutive doses of about 200 μL, was deposited on the surface of the PS dishes. After the last dose, the sample was left on the spin-coater for another 120 s. Unless otherwise stated, all of the experiments were performed at the temperature of 295 K (substrate, solutions, and surrounding atmosphere). Moreover, the air humidity was monitored and kept at (50 ± 2)%.

Plasma Surface Modification. To increase the affinity of the cultivated cells to the surface, the unmodified and modified PS Petri dishes were pretreated with a low-temperature air plasma. The treatment was performed in a Diener PICO plasma apparatus (Diener electronic GmbH + Co.KG) with capacitive radiofrequency coupling at the frequency of 13.56 MHz and a pressure of 0.4 mbar. The following procedure was utilized: the substrates were placed inside the plasma chamber, and then the vacuum pump was activated; after 5 min, the chamber was purged with air (purity 99.999%) at 10 sccm for another 5 min to minimize the effect of contaminants possibly present in the chamber. Subsequently, the air flow was adjusted to 5 sccm, and the discharge was initiated. The forward power was set to 100 W, and the reflected power was kept under 10% with the help of the matching circuit during all experiments. Beside this, the peripheries of the PS dishes were activated with the PlasmaBeam^{DUO}PC (Diener) for 3 s at a power of 100 W to enhance the excess solvent drain off. After treatment, the substrates were kept in a desiccator at a constant temperature of 298 K.

Surface Characterization and Scanning Electron Microscopy. Changes in the surface appearance were analyzed by a scanning electron microscope (SEM), model Phenom Pro (Phenom-World BV). The samples were observed at the acceleration voltage of 10 kV in the backscattered electron mode with magnifications of 2000−4000×. Measurements were carried out on samples without prior metallization using a special sample holder that allows the reduction of charges on nonconductive materials.

The distribution of pore areas was obtained by image analysis with the ImageJ 1.5 software (Wayne Rasband, National Institutes of Health, United States).

Profilometry. Changes in the surface roughness were characterized by contact and noncontact profilometers, using Bruker Nano's Contour model GT-K and DektakXT. A diamond tip with a radius of curvature of 2.5 μm and a pressure equivalent of 5 mg was used to make measurements with the contact profilometer. The measurements on the noncontact profilometer were conducted using white light and a lens with a magnification of 20×. The evaluation of the surface roughness was performed according to the ASME B46.1 standard.

Atomic Force Microscopy. Changes in the surface topography were characterized using the atomic force microscope (AFM), model Dimension ICON (Bruker). Measurements were performed at the scan speed of 0.5 Hz with a resolution of 512 × 512 pixels in the tapping mode at room temperature in air atmosphere. A silicone-nitride probe with a resonant frequency of (150 ± 50) kHz and a stiffness constant of 5 N/m (MPP-12120, Bruker) was used.

Goniometry. The contact angle of water (θ) on the treated PS surface was characterized with a homemade goniometer with the DropCA software v1.05 (BLI Instruments) for automatic image analysis. Measurements were performed at room temperature (298 ± 1) K. A drop with a volume of 3 μL was deposited on the measured surface. Ultrapure water with the resistance of 18.2 MΩ·cm was used for the measurement. All measurements were repeated 10 times; the mean values and standard deviations are presented in the results.

Cell Adhesion and Proliferation. Prior to in vitro testing, the samples were disinfected by 30 min of exposure to a UV−radiation source operating at a wavelength of 258 nm, emitted from a low-pressure mercury lamp. The influence of structured surfaces on the mouse embryonic fibroblast NIH/3T3 cell line (ATCC; US) was investigated. Cell adhesion was evaluated after 1 and 3 h, and proliferation was evaluated after 48 h. ATCC-formulated Dulbecco's modified Eagle's medium (Biosera; France) containing 10% calf serum (Biosera; France) and 100 U·mL^{-1} penicillin/streptomycin (PAA; Switzerland) was used as the culture medium.

The cells were seeded on the reference culture dishes (TPP; Switzerland) and the structured surfaces in the concentration of 1 × 10^6 cells mL^{-1}. After 3 h, the cells were gently rinsed, and micrographs were taken using an Olympus IX51 microscope (Olympus, Japan).

Cell proliferation and morphology were evaluated on the cells seeded at the initial concentration of 1 × 10^5 cells mL^{-1} after 48 h of cultivation. The proliferation was evaluated by an MTT assay. The impact of cultivation on the structured surfaces of cell cytoskeletons was evaluated using an ActinRed 555 (Thermo Fisher Scientific,

DOI: 10.1021/acsami.6b15774
ACS Appl. Mater. Interfaces 2017, 9, 6472−6481

United States). The proliferated cells were first fixed using 4% formaldehyde (Penta, Czech Republic) for 15 min, washed by a PBS buffer, and subsequently poured with a 0.5% Triton X-100 (Sigma-Aldrich, United States) for 5 min until permeabilization. The required amount of PBS, one drop per 1 mL of ActinRed 555, was added and left to incubate for 30 min in the dark.

RESULTS AND DISCUSSION

Influence of the Time Sequence of Dosing the Solvent onto the PS Substrate. The experimental results showed that dividing comparable amounts of the good and poor solvent blends intended for PS surface modification into several smaller doses allowed significant modification of the appearance and wetting properties of the surface (Figure 1). When the solvent blend was dosed on the PS surface in one step (1 × 1000 μL), a surface with microcracks and a smaller number of 5−10 μm deep pores was obtained (Figures 1B and D). Application of a sequenced dosing (5 × 200 μL, each 5 s) led to a much more compact surface with a large amount of big pores with various diameters and depths up to 5 μm (Figures 1C and D). The number of pores and their surface distributions changed significantly (Figure 1D). To explain such changes, a number of variables should be considered: sample rotation at 2200 rpm, polymer swelling, surface dissolution, phase separation,[2,33] division of the system into elastic, viscoelastic, and viscous parts, the generation of secondary flows based on the concentration-diffusional mechanism related to rapid viscosity changes during solvent evaporation,[37−39,46] surface free tension, and interfacial tension.[34,35]

Critical Parameters of the PS Surface Modification Process. Importantly, the material was treated under dynamic conditions during the spin-coating process, which allowed for the rapid and uniform coverage of the surface with the solvent blend. Thus, almost 80% of the treated surface area exhibits comparable surface relief. The peripheral area, close to the edges, was excluded from the analysis because of the accumulation of solvents and artifacts resulting from residual stresses in the substrate material.

Specific deformation of the pores (Figures 1B and C) can be attributed to centrifugal forces and directional air flow above the surface.[47] Also, the viscoelastic phase separation defined by Tanaka[21,33] should be considered. The presence of small micropores among the large ones in Figure 1C can be viewed as the tendency of the system to maximize the volume infilling, accompanied by the fact that not all droplets have undergone the coalescence process in the rapid (total time 20 s) process of PS surface topography modification. The generated pores do not exhibit narrow dimension distribution (Figures 1D, 3D, and 6C), as would be expected in the case of the breath figures approach. This fact can be attributed to the overcoming of the time threshold value related to the growth of the poor solvent droplets and the subsequent coalescence, as described in the literature.[1] Upon comparing our pore size distributions (Figures 1D, 3D, and 6C) with the results presented elsewhere,[1,7,32,35,48,49] we can conclude that our approach allows for the preparation of a wide spectrum of porous surfaces, ranging in pore sizes from one millimeter to hundreds of square millimeters.

The choice of the good/poor solvent system was based on these requirements: the components have to be mutually miscible, and the good solvent evaporation rate has to be much higher than that of the poor one to allow the fixation of surface pores, similar to that in the breath figures approach.[1,31] On the basis of the Hansen solubility parameter[7] and the initial experiments, the combination tetrahydrofuran (THF, good solvent) and 2-ethoxyethano (ETH, poor solvent) was chosen for the PS surface modification. The mutual THF:ETH ratio is an important parameter, along with the sequential dosing of the mixture. The effect of relative humidity, which can significantly affect the process of pore generation,[32,48] was minimized in our experiments by maintaining constant environmental conditions.

The process is further affected by gradual THF evaporation from the swollen PS and ETH microdroplets. If the process ended after the first deposition step, no substantial surface microstructure could be observed (Figure 2A). A several-fold

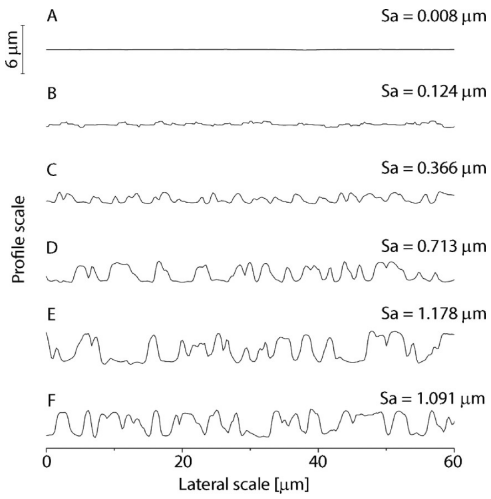

Figure 2. PS surface evolution as a function of solvent mixture dose number. (A) Single dose, (B) 2 doses, (C) 4 doses, (D) 6 doses, (E) 8 doses, and (F) 10 doses. One dose equals 200 μL of the THF:ETH 1.1:8.9 mixture. Interval of 5 s between the doses at 295 K. Profiles obtained with optical profilometer. Respective surface roughness (Sa) is displayed for each profile.

repetition of the 200 μL deposition steps with a 1.1:8.9 volume ratio of THF:ETH results in an increase of pore size and depth (Figures 2B−F). The maximal modification was reached after eight steps with no further changes observed. The pore diameter:depth ratio approaches 1 after 8 and more steps (Figures 2E and F). Duration of the time sequence determines the number and size of surface pores. Prolongation of the sequence between steps from 5 to 10 s results in a lower number of pores with higher diameters (Figures 3A, B, and D). Almost no significant pores were observed on the surface when the sequence was further prolonged to 20 s (Figure 3C). These microstructural changes are accompanied by the gradual change of the contact angle values and clearly demonstrate the well-known effect[13,14] of the surface structure on the wetting properties of surfaces (Figures 3A−C).

The experimental results presented in Figure 4 demonstrate that a twice-repeated deposition (in total 10 × 200 μL, each 5 s) has a similar effect as dosing 5 × 200 μL, each 10 s; see the comparison in Figures 3B and 4B. This fact could possibly be attributed to the change of the specific surface area that in turn defines the THF penetration rate into the PS substrate and thus the depth of the swollen layer. Finally, the swollen layer depth determines the aggregation extent of separated ETH micro-droplets. The pores created in the initial steps also allow more solvent to be trapped there, even under rotation, and contribute to the creation of sufficiently thick, mobile PS/THF layer.

DOI: 10.1021/acsami.6b15774
ACS Appl. Mater. Interfaces 2017, 9, 6472−6481

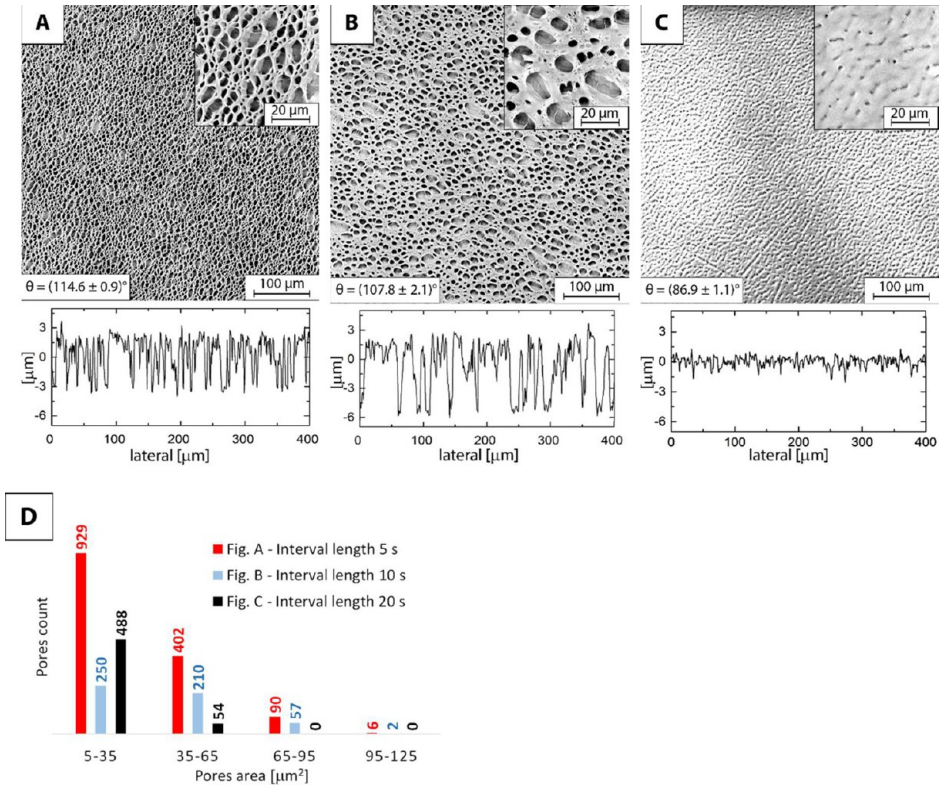

Figure 3. Effect of the dosing interval length on the PS surface topography. Interval lengths: (A) 5 s, (B) 10 s, and (C) 20 s. In total, five doses of 200 μL of the THF:ETH 1.25:8.75 mixture were deposited at 295 K. SEM images with respective water contact angle values. Under each image, the respective surface profile is displayed (obtained with a contact profilometer). Pore area distribution in the square 268 × 268 μm is displayed in panel D.

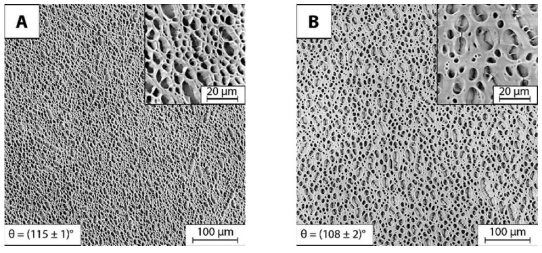

Figure 4. Effect of repeated modification on the topography of PS surfaces. (A) first modification, (B) subsequent modification. Each modification performed at the same conditions: 5 s time interval of depositing 5 doses, each 200 μL of the THF:ETH 1.5:8.5 mixture at 295 K. SEM images with respective water contact angle values.

Thus, the longer interval between the THF/ETH dosing steps (steps 1 and 2 in Figure 7) provides the system enough time to form a thicker swollen surface layer and results in the related aggregation of the individual microdroplets into larger units (see the interval 10 s in Figure 3B) or in solvent evaporation (see the interval 20 s in Figure 3C).

Effect of the Mixture Component Ratio on the PS Surface Relief. The ratio THF:ETH 1:9 (Figure 5A) results in a surface with pores about 1 μm in diameter and tens to hundreds of nanometers deep, as a consequence of a too-thin swollen layer PS/THF and thus a limited coalescence of ETH microdroplets. The predominantly elastic swollen PS layer does not allow embossing of the droplet under the action of Laplace pressure (surface, interfacial tension).[34,35]

A 5% increase in the good solvent concentration (THF:ETH 1.5:8.5) changes the situation dramatically (Figure 5B). A suitable amount of good solvent is present in the system, allowing the creation of sufficiently thick and moderately mobile swollen surface layer. Such a layer can evolve into a specific network structure with increased hydrophobicity (θ = (110 ± 3)°) when an appropriate time sequence dosing is applied. The reason for such a network-like phase separation, as defined by Tanaka,[33] is related to the fact that for a limited time the deformation component dominates the relaxation one in the system, and the polymer can reorganize while the separation of the poor solvent takes place. Another increase in the THF:ETH ratio 2:8 (Figure 5C) shifts the whole system further in the imaginary phase diagram, where the network character of the structure is no longer observed. Instead, mainly pores with large diameters and depths can be observed, as during their formation the Laplace pressure could fully dominate, and the droplets adopted a shape representing the lowest possible surface energy. This type of surface resembles the sponge-like phase separation in the form of isolated cells.[33] The creation of such a pattern is closely connected with the presence of a sufficient amount of the good solvent in the mixture, which allows the formation of a thick swollen layer where viscous behavior dominates the elastic. Thus, the coalescence process of the poor solvent droplets can proceed (compare Figure 5A to 5D) along with the material flow driven by the concentration differences arising due to good solvent rapid evaporation.[38,39] Relics of these flows, presented as a specific surface corrugation and residual stresses in the polymer matrix, can be observed in the AFM phase contrast images (Figure 6, right).

Further increasing the good solvent ratio (Figures 5D and E) causes additional poor solvent aggregation followed by the

DOI: 10.1021/acsami.6b15774
ACS Appl. Mater. Interfaces 2017, 9, 6472−6481

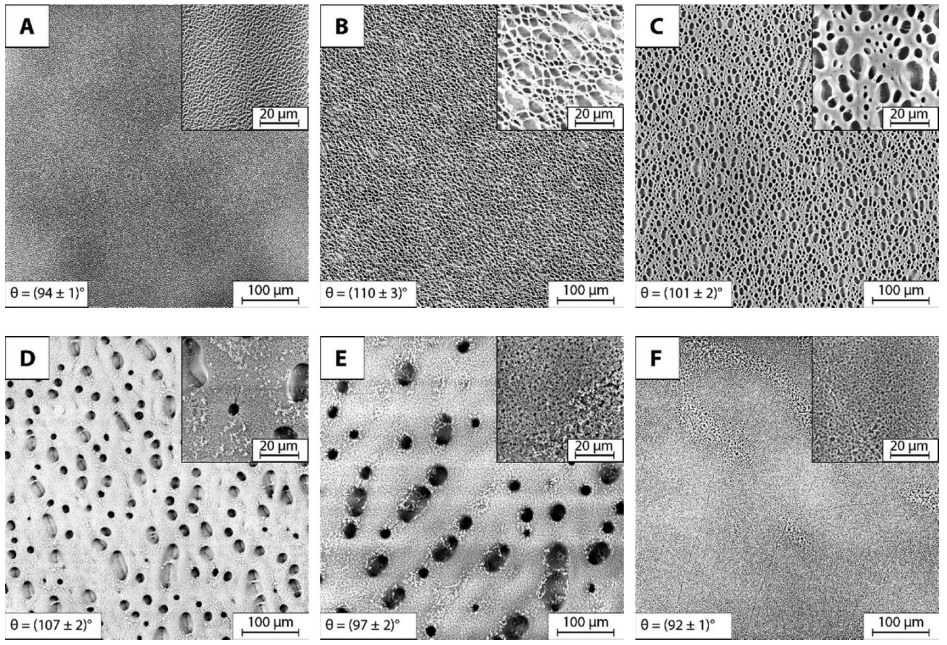

Figure 5. Effect of the THF:ETH ratio on the PS surface topography. Volume ratios of THF:ETH: (A) 1:9, (B) 1.5:8.5, (C) 2:8, (D) 3:7, (E) 5:5, and (F) 7:3. Five second time interval of depositing 5 doses, each 200 μL at 295 K, were used. SEM images with respective water contact angle values.

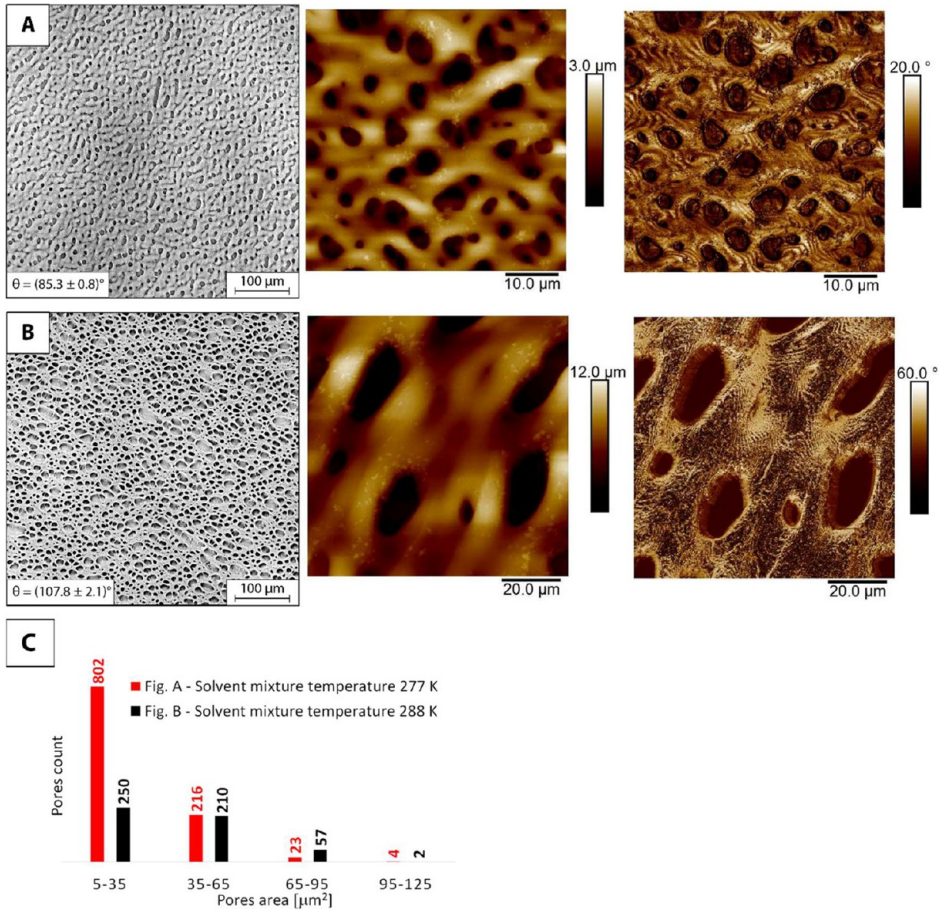

Figure 6. Effect of temperature on the PS surface topography. The volume ratio of THF:ETH was 2:8. The solvent mixture temperature at (A) 277 and (B) 288 K. Five second time intervals of depositing 5 doses, each 200 μL, were used. SEM image with respective water contact angle value (left), AFM topography image (middle), AFM phase contrast image (right). Pore area distribution in the square 268 × 268 μm is displayed in panel C.

DOI: 10.1021/acsami.6b15774
ACS Appl. Mater. Interfaces 2017, 9, 6472−6481

formation of macrodroplets, resulting in a gradually lower number of large pores at the surface which completely disappear once the THF:ETH ratio reaches 7:3 (Figure 5F). Visible corrugation in Figure 5F can arise due to the rapid evaporation of the good solvent from the thin swollen layer without the presence of the poor solvent, as documented in the literature.[37,39,50]

The apparent similarity of the surface in Figure 5F to the initial condition in Figure 5A can be explained by the creation of a very mobile layer of dissolved PS containing a smaller amount of the poor solvent. The poor solvent with the dissolved PS was then transferred to the outskirts of the PS dish due to the action of the centrifugal force. It means that in every step, only a partially swollen PS layer is modified simulating low dosing experiments in Figure 2B.

Interestingly, an increase in the water contact angle can be observed in Figure 5D. Such a drop in the surface free energy of the substrate can be attributed to PS microaggregates (Figures 5D and E) which, along with the deep pores, form a hierarchically structured surface, which is necessary to reach the self-cleaning effect.[13]

Effect of Solvent Temperature on the PS Surface Relief Development. The previously discussed experiments were performed at the room temperature (295 K) of both the solvent mixture and the PS surface. Virtually all parameters, i.e., character of the polymer system, THF/PS diffusion rate, THF and ETH evaporation rates, viscosity, etc., are temperature-dependent. Temperature and its variations can generate specific flows,[36,38,40,41] resulting in polymer matrix rearrangement and the related fixation of residual stresses in the PS surface layer; see the AFM phase contrast image in Figure 6.

In these experiments, a series of 5 drops of colder solvent mixtures (277 or 288 K) were deposited on the PS substrate (295 K). The deposition of a cold solvent onto a surface with an elevated temperature was immediately followed by the solvent heating and surface cooling and led, along with the repetition of this step and concentration gradients in the polymer surface layer, to the evolution of the organized liquid flow in the upmost viscoelastic PS layer. An action resembling the Bénard–Marangoni convection[39,50] can be observed in the AFM phase-contrast images as contour lines surrounding individual pores. The variations in diameter and depth of the pores in the matrix (Figures 6A–C) can be explained as follows. The solvent with a lower temperature (277 K) will cool the PS substrate more significantly, and simultaneously, the THF cannot penetrate deeply enough to form a sufficiently thick swollen layer that allows for the embossing of the ETH droplets into the substrate and the aggregation of ETH into larger units, as opposed to the situation with the solvent at a temperature of 288 or 295 K.

Surface Microstructure Evolution. Figure 7 schematically demonstrates the process of surface relief evolution during the process of the sequential deposition of the THF: ETH mixture. In the first step (Figure 7A), 200 μL of the mixture (1 to 2:8 to 9 volume ratio THF:ETH) is dosed, and the THF immediately penetrates the PS surface, which swells and further dissolves if more THF is added (3 and more: 7 and less THF:ETH volume ratio). Along with preferential THF evaporation, the ETH phase separation occurs in the form of small ETH micro-droplets (Figure 7B). These droplets naturally tend to form a spherical shape (minimum surface energy), which helps their embossing into the swollen PS surface layer. In the final stage of this step, Figure 7C, when only ETH stays at the surface and

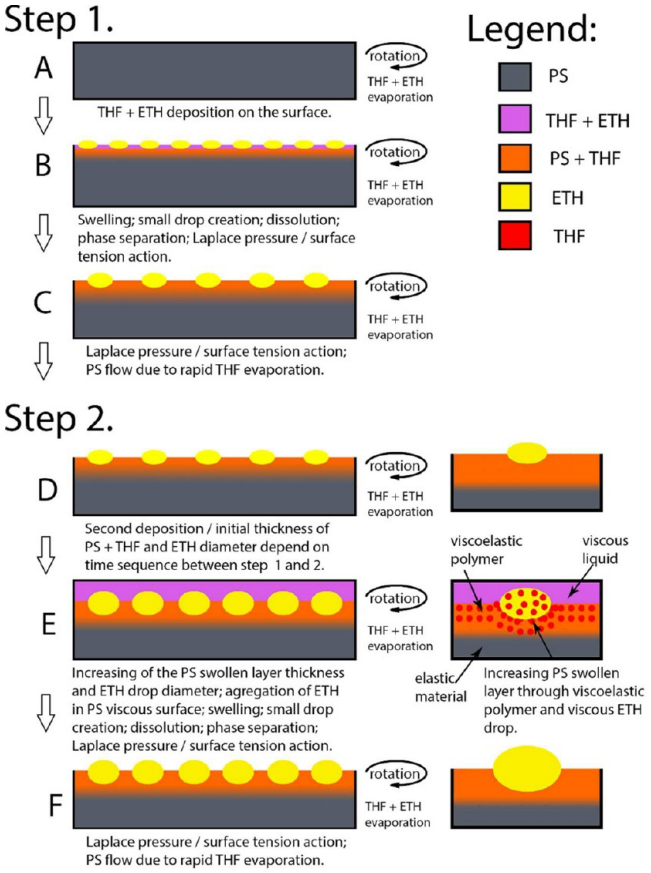

Figure 7. Model of PS surface modification with micropores due to the time sequenced dosing of the good/poor solvent mixture. For simplicity, only the processes occurring between the first and second dosing steps are displayed. Further steps repeat accordingly. Individual stages of the experiment (A–F) are described in the text.

THF is present in the swollen PS layer, the further embossing of the microdroplets into the viscoelastic surface layer occurs due to the Laplace pressure, as described in the literature.[34]

Repeated additions of the solvent mixture onto the surface consisting of microdroplets of a poor solvent and swollen polymer layer (Figure 7D) result in an increase of the swollen layer depth, migration, aggregation (coalescence process), and growth of the separated ETH microdroplets (Figure 7E). The ETH microdroplet aggregation is only allowed with the increasing thickness of the swollen layer, which exhibits a viscous behavior in its upper part and gradually changes to viscoelastic with depth. Inserts in Figures 7D–F suggest a mechanism of good solvent diffusion under the ETH microdroplet. This model assumes that the THF transport, driven by the diffusion mechanism, occurs not only through the swollen PS layer but also through the ETH volume, as illustrated in the insets in Figure 7E. In the final stage of this step (Figure 7E), the surface consists of a swollen PS layer and large ETH droplets which do not contain THF. The process of PS surface forming is connected with the following phenomena in this step: diffusion of the THF into PS, growth of the PS swollen layer, viscoelastic phase separation, the reforming (aggregation) of the ETH microdroplets, the embossing of the ETH microdroplets into the PS surface forced by the Laplace pressure, deformation of the droplets' shape, evaporation of the individual solvents from the mixture, and surface relief fixation. As discussed, the deformation of the originally spherical

DOI: 10.1021/acsami.6b15774
ACS Appl. Mater. Interfaces 2017, 9, 6472–6481

micropores in the PS surface is related to the sample rotation, rapid air flow,[47] viscoelastic character of the system,[21,33] internal stresses in the polymer matrix,[7] and the time sequence of individual deposition steps, as shown in Figure 3.

Our approach is simple, robust, and rapid. The fixation of a relief occurs during tenths of a second between the solvent mixture deposition and its evaporation. The treated surface does not have to be pretreated or conditioned, there is no need for preparing mixtures of polymer solutions, the presence of other supporting structures, the use of a special apparatus for controlling the changes in the air humidity, vapor pressure, the air convection rate above the surface, etc., as in other methods[1,2,7,31,32,34,35,51]

Wettability of Surfaces Designed for Cell Cultivation. As described in the literature, specifically structured surfaces can be utilized for cell cultivation (they can mimic different components of an extracellular matrix and therefore provide different impulses for the cells).[7,8,18,43−45] The surface displayed in Figure 3A was used for such experiments. The textured PS surfaces were first plasma treated to modify their surface characteristics from hydrophobic to hydrophilic (Table 1). As

Table 1. Water Contact Angle Values of Original (PS) and Modified (M-PS) Petri Dishes[a]

sample	plasma treatment time (s/W)	water contact angle (deg)	
		1 h after plasma treatment	1 h after plasma treatment and 30 min UV sterilization
PS		78 ± 2	80 ± 1
PS-50W	2/50	24 ± 2	53 ± 1
PS-100W	3/100	13 ± 1	40 ± 1
M-PS		106 ± 2	104 ± 1
M-PS-20W	2/20	79 ± 5	93 ± 4
M-PS-50W	2/50	43 ± 4	82 ± 4
M-PS-100W	3/100	34 ± 2	67 ± 5

[a]Modification with a 5 × 200 μL of THF:ETH 1.25:8.75 mixture, deposition interval 5 seconds. Subsequently, the surfaces were plasma-treated, sterilized, and modified with a cultivation medium. All experiments and measurements, excluding the application of a culture media, were performed at 295 K.

can be observed, the contact angles decrease with more intense plasma treatment (Table 1). For textured surfaces, however, this decrease is not as significant as that for the unmodified PS because the microstructuring inherently increases the hydrophobicity of the surfaces (lotus effect). The subsequent UV sterilization does not have a substantial effect on the wetting characteristics of nontreated samples. This is important, as the impact of sterilization on the surface properties of any material can limit its applicability as a biomaterial. In contrast, the plasma-treated samples exhibit a significant increase in the contact angles almost to the initial value for the nontreated surface. This can be attributed to the reaction of the functional groups induced during the plasma treatment with the UV-initiated byproducts from air, moisture, and organic impurities. Also, the plasma-treated samples alone are subjected to the phenomenon called aging: a gradual process of deterioration of the properties of the modified surface layer. Aging is explained in terms of the reorientation of functional groups incorporated at plasma treatment during time intervals and also by the adverse effects of elevated humidity and temperature.[42] Various attempts to retard this so-called "hydrophobic recovery" have been reported.[52−56] The surfaces of plasma-treated Petri dishes exhibit the signs of aging as well (Figure 8). On the other hand, this recovery is not very significant, and in most cases the

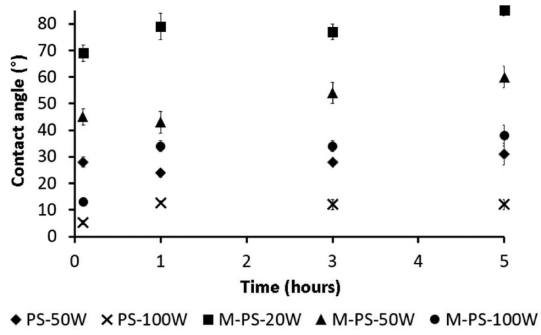

Figure 8. Contact angle of water on plasma-treated PS surface as a function of aging time.

contact angle change stays below 10° after 3 h of aging. It should be mentioned that the experiments with cell proliferation and adhesion were performed within a 2h interval after the PS surface plasma treatment and thus were not significantly affected by the aging of the treated surface.

Cell Adhesion and Proliferation on Structured Surfaces. The surface properties of materials can significantly influence cell adhesion, proliferation, differentiation, and gene expression, as discussed above.[7,8,18,43−45] Figure 9 displays adhered cells on referential (PS) and structured (M-PS) surfaces without plasma pretreatment.

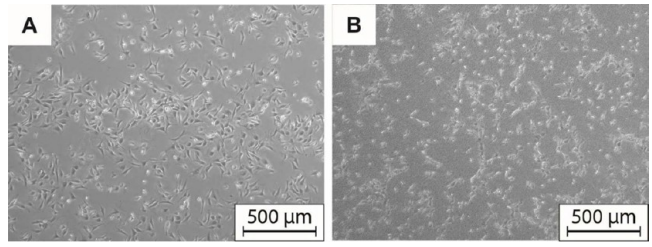

Figure 9. Adhesion of NIH/3T3 determined 3 h after seeding on (A) reference PS and (B) M-PS; all of the other surfaces prove similar adhesions as reference (optical microscope images).

The number of viable cells (Figure 10) was lower on M-PS, M-PS-20W, and M-PS-50W compared to that on the reference PS.

Cell viability (Figure 10) is, however, only one parameter of the cell's behavior. Cytoskeleton structure is another important factor that can indicate if the cell is under a physiological condition. It is known that on flat surfaces, the cytoskeleton structure and orientation are changed compared to the in vivo state (e.g., the number of stress fibers is significantly increased in the case of fibroblasts). Considering the practical application of any biomaterial, the impact on cytoskeleton is therefore at the center of attention. The impact of topography on the cytoskeleton formation was detected by actin staining. From the micrographs presented in Figure 11, it can be concluded that the cytoskeletons of cells cultivated on samples PS-50W and M-PS-20W are similar to those in the reference PS.

Despite the dramatic change of topography (samples marked M-PS), the cytoskeletal structure does not change significantly with moderate hydrophilicity increase (plasma treatment 20 W). At more hydrophilic surfaces (plasma treatment 100 W for

DOI: 10.1021/acsami.6b15774
ACS Appl. Mater. Interfaces 2017, 9, 6472−6481

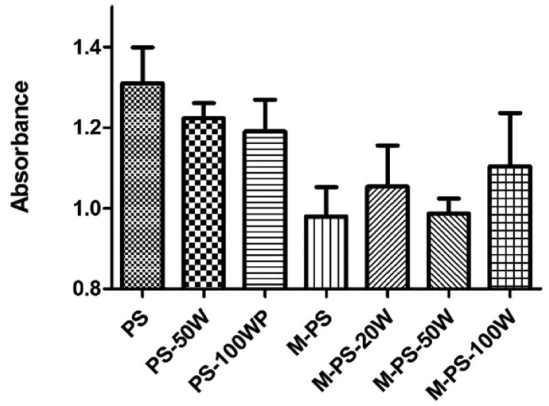

Figure 10. Number of viable cells determined by MTT assay and expressed as average absorbance and its standard deviation.

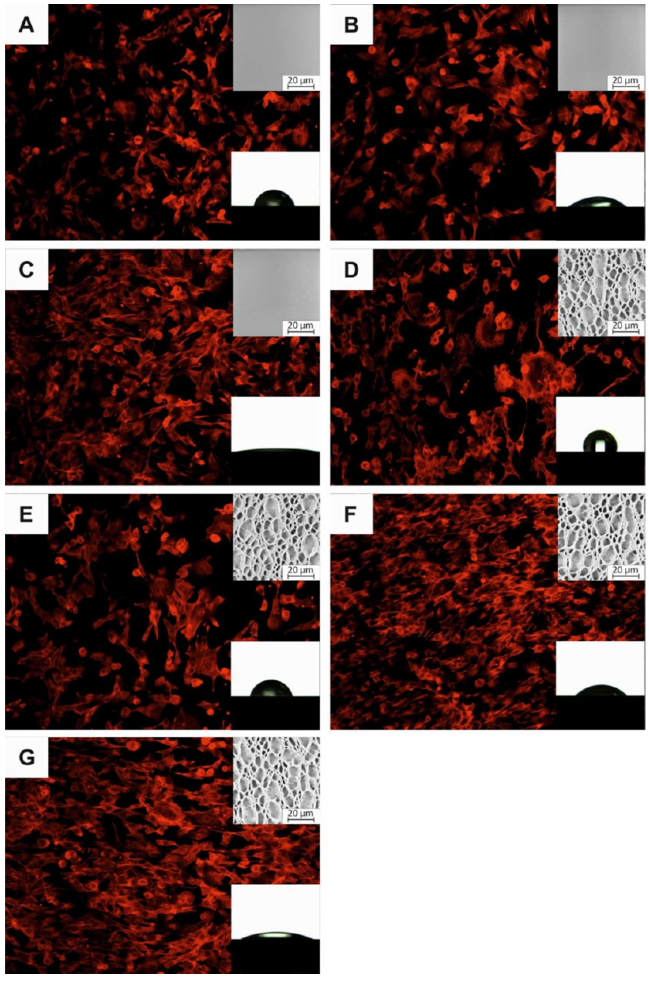

Figure 11. Cytoskeleton of NIH/3T3 visualized by ActinRed on (A) reference PS, (B) PS-50W, (C) PS-100WP, (D) M-PS, (E) M-PS-20W, (F) M-PS-50W, and (G) M-PS-100W. Top-right corner: SEM image of the used surface; bottom-right corner: water drop on the studied surface as a measure of surface hydrophility.

PS and 50/100 W for M-PS), the cell's cytoskeleton is altered noticeably at both substrates: the referential PS and modified M-PS. This suggests that the surface energy plays a primary role, and the surface relief plays a secondary role, probably because the structured and (at the same time) hydrophilic surfaces better mimic the native 3D structure of biological tissue.

In the case of surfaces M-PS and M-PS-20W, the cells are more compact, spherical, and create filopodia. On the M-PS-50W and M-PS-100W surfaces, the cells seems to be preferentially oriented, and their morphology is closer to the normal fibroblast morphology on planar surfaces. It can therefore be concluded that, based on both the cell viability as well as cell morphology experiments, the M-PS-100W is the most promising surface for biological applications.

CONCLUSIONS

The factors determining the evolution of PS-based structured surfaces were examined. The PS substrate modification was performed in a spin-coater with a good/poor solvent mixture to achieve a homogeneous surface texture. Although the overall process includes complex factors such as diffusion, swelling, viscoelastic phase separation, surface tension variation, action of inertial forces, solvent evaporation, and the generation of secondary flows via concentration and temperature differences, the texturing itself could by controlled by a simple dosing sequence of the solvent mixtures. The proper control of this variable, along with the volume and number of the doses, allows the preparation of a wide spectrum of structured surfaces without modifying the discussed physicochemical parameters. Surface modifications, from the network structures to the isolated micropores, can be achieved. The micropore aspect ratio can be further modified by varying the number of subsequently deposited doses. The type, number, and dimensions of the micropores are closely related to the initial texture of the treated surface (its specific surface area) and are affected by the rate at which the swollen layer, allowing the formation of micropores, evolves. The secondary flows occurring at the surface layer induce residual stress at the micropore borders, as observed by AFM.

The presented method allows the cheap and reproducible preparation of a broad range of microstructured PS surfaces. These properties make the presented system ideal for the large-scale preparation of culture substrates for studies of surface topography influence on cell cultivation. Moreover, the polystyrene surfaces can be easily further modified in terms of their surface energy, allowing various biologically active molecules to bind.

AUTHOR INFORMATION

Corresponding Author

*E-mail: minarik@ft.utb.cz.

ORCID

Antonín Minařík: 0000-0002-0055-675X

Notes

The authors declare no competing financial interest.

ACKNOWLEDGMENTS

This article was written with the support of the Operational Program Research and Development for Innovations cofunded by the European Regional Development Fund (ERDF) and the national budget of the Czech Republic within the framework of the project Centre of Polymer Systems (reg. number: CZ.1.05/2.1.00/03.0111). This work was supported by the Ministry of Education, Youth and Sports of the Czech Republic, Program NPU I (LO1504) and by the European Regional Development Fund (Grant CZ.1.05/2.1.00/19.0409) as well as by TBU

DOI: 10.1021/acsami.6b15774
ACS Appl. Mater. Interfaces 2017, 9, 6472−6481

Grants IGA/FT/2015/014 and IGA/FT/2016/013 funded by the resources of specific university research.

REFERENCES

(1) Munoz-Bonilla, A.; Fernandez-Garcia, M.; Rodriguez-Hernandez, J. Towards Hierarchically Ordered Functional Porous Polymeric Surfaces Prepared by the Breath Figures Approach. *Prog. Polym. Sci.* **2014**, *39* (3), 510−554.

(2) Xue, L. J.; Zhang, J. L.; Han, Y. C. Phase Separation Induced Ordered Patterns in Thin Polymer Blend Films. *Prog. Polym. Sci.* **2012**, *37* (4), 564−594.

(3) Xu, Y.; Zhu, X.; Dan, Y.; Moon, J.; Chen, V.; Johnson, A.; Perry, J.; Yang, S. Electrodeposition of Three-Dimensional Titania Photonic Crystals from Holographically Patterned Microporous Polymer Templates. *Chem. Mater.* **2008**, *20* (5), 1816−1823.

(4) Kyu, T.; Nwabunma, D. Simulations of Microlens Arrays Formed by Pattern-Photopolymerization-Induced Phase Separation of Liquid Crystal/Monomer Mixtures. *Macromolecules* **2001**, *34* (26), 9168−9172.

(5) Campoy-Quiles, M.; Ferenczi, T.; Agostinelli, T.; Etchegoin, P.; Kim, Y.; Anthopoulos, T.; Stavrinou, P.; Bradley, D.; Nelson, J. Morphology Evolution via Self-Organization and Lateral and Vertical Diffusion in Polymer: Fullerene Solar Cell Blends. *Nat. Mater.* **2008**, *7* (2), 158−164.

(6) Li, L.; Chen, C.; Li, J.; Zhang, A.; Liu, X.; Xu, B.; Gao, S.; Jin, G.; Ma, Z. Robust and Zydrophilic Polymeric Films with Honeycomb Pattern and Their Cell Scaffold Applications. *J. Mater. Chem.* **2009**, *19* (18), 2789−2796.

(7) DeRosa, M.; Hong, Y.; Faris, R.; Rao, H. Microtextured Polystyrene Surfaces for Three- Dimensional Cell Culture Made by a Simple Solvent Treatment Method. *J. Appl. Polym. Sci.* **2014**, *131* (14), 1.

(8) Flemming, R.; Murphy, C.; Abrams, G.; Goodman, S.; Nealey, P. Effects of Synthetic Micro- and Nano-Structured Surfaces on Cell Behavior. *Biomaterials* **1999**, *20* (6), 573−588.

(9) Martinez-Campos, E.; Elzein, T.; Bejjani, A.; Garcia-Granda, M.; Santos-Coquillat, A.; Ramos, V.; Munoz-Bonilla, A.; Rodriguez-Hernandez, J. Toward Cell Selective Surfaces: Cell Adhesion and Proliferation on Breath Figures with Antifouling Surface Chemistry. *ACS Appl. Mater. Interfaces* **2016**, *8* (10), 6344−6353.

(10) Tanev, P.; Chibwe, M.; Pinnavaia, T. Titanium-Containing Mesoporous Molecular-Sieves for Catalytic Oxidation of Aromatic Compounds. *Nature* **1994**, *368* (6469), 321−323.

(11) Aizenberg, J.; Black, A.; Whitesides, G. Control of Crystal Nucleation by Patterned Self-Assembled Monolayers. *Nature* **1999**, *398* (6727), 495−498.

(12) De Leon, A.; Garnier, T.; Jierry, L.; Boulmedais, F.; Munoz-Bonilla, A.; Rodriguez-Hernandez, J. Enzymatic Catalysis Combining the Breath Figures and Layer-by-Layer Techniques: Toward the Design of Microreactors. *ACS Appl. Mater. Interfaces* **2015**, *7* (22), 12210−12219.

(13) Bhushan, B.; Jung, Y. C.; Koch, K. Self-Cleaning Efficiency of Artificial Superhydrophobic Surfaces. *Langmuir* **2009**, *25* (5), 3240−3248.

(14) Brown, P.; Talbot, E.; Wood, T.; Bain, C.; Badyal, J. Superhydrophobic Hierarchical Honeycomb Surfaces. *Langmuir* **2012**, *28* (38), 13712−13719.

(15) Manabe, K.; Nishizawa, S.; Shiratori, S. Porous Surface Structure Fabricated by Breath Figures that Suppresses Pseudomonas aeruginosa Biofilm Formation. *ACS Appl. Mater. Interfaces* **2013**, *5* (22), 11900−11905.

(16) Walheim, S.; Schaffer, E.; Mlynek, J.; Steiner, U. Nanophase-Separated Polymer Films as High-Performance Antireflection Coatings. *Science* **1999**, *283* (5401), 520−522.

(17) Schottner, G. Hybrid Sol-Gel-Derived Polymers: Applications of Multifunctional Materials. *Chem. Mater.* **2001**, *13* (10), 3422−3435.

(18) Tserepi, A.; Gogolides, E.; Bourkoula, A.; Kanioura, A.; Kokkoris, G.; Petrou, P. S.; Kakabakos, S. E. Plasma Nanotextured Polymeric Surfaces for Controlling Cell Attachment and Proliferation: A Short Review. *Plasma Chem. Plasma Process.* **2016**, *36* (1), 107−120.

(19) Jianfeng, L.; Dornfeld, D. A. Material Removal Mechanism in Chemical Mechanical Polishing: Theory and Modeling. *IEEE Int. Symp. Semicond. Manuf.* **2001**, *14* (2), 112−133.

(20) Han, J. T.; Xu; Cho, K. Diverse Access to Artificial Superhydrophobic Surfaces Using Block Copolymers. *Langmuir* **2005**, *21* (15), 6662−6665.

(21) Tanaka, H. Formation of Network and Cellular Structures by Viscoelastic Phase Separation. *Adv. Mater.* **2009**, *21* (18), 1872−1880.

(22) Bui, V.; Ko, S.; Choi, H. Large-Scale Fabrication of Commercially Available, Nonpolar Linear Polymer Film with a Highly Ordered Honeycomb Pattern. *ACS Appl. Mater. Interfaces* **2015**, *7* (19), 10541−10547.

(23) Shojaie, S. S.; Krantz, W. B.; Greenberg, A. R. Dense Polymer Film and Membrane Formation via the Dry-Cast Process Part I. Model Development. *J. Membr. Sci.* **1994**, *94* (1), 255−280.

(24) Shojaie, S. S.; Krantz, W. B.; Greenberg, A. R. Dense Polymer Film and Membrane Formation via the Dry-Cast Process Part II. Model Validation and Morphological Studies. *J. Membr. Sci.* **1994**, *94* (1), 281−298.

(25) Altinkaya, S. A.; Ozbas, B. Modeling of Asymmetric Membrane Formation by Dry-Casting Method. *J. Membr. Sci.* **2004**, *230* (1−2), 71−89.

(26) Matsuyama, H.; Nishiguchi, M.; Kitamura, Y. Phase Separation Mechanism During Membrane Formation by Dry-Cast Process. *J. Appl. Polym. Sci.* **2000**, *77* (4), 776−783.

(27) Onuki, A. Late Stage Spinodal Decomposition in Polymer Mixtures. *J. Chem. Phys.* **1986**, *85* (2), 1122−1125.

(28) Samuel, A.; Umapathy, S.; Ramakrishnan, S. Functionalized and Postfunctionalizable Porous Polymeric Films through Evaporation-Induced Phase Separation Using Mixed Solvents. *ACS Appl. Mater. Interfaces* **2011**, *3* (9), 3293−3299.

(29) Li, W.; Ryan, A. J.; Meier, I. K. Morphology Development via Reaction-Induced Phase Separation in Flexible Polyurethane Foam. *Macromolecules* **2002**, *35* (13), 5034−5042.

(30) Matsuzaka, K.; Jinnai, H.; Koga, T.; Hashimoto, T. Effect of Oscillatory Shear Deformation on Demixing Processes of Polymer Blends. *Macromolecules* **1997**, *30* (4), 1146−1152.

(31) Bunz, U. H. F. Breath Figures as a Dynamic Templating Method for Polymers and Nanomaterials. *Adv. Mater.* **2006**, *18* (8), 973−989.

(32) Huang, C.; Kamra, T.; Chaudhary, S.; Shen, X. Breath Figure Patterns Made Easy. *ACS Appl. Mater. Interfaces* **2014**, *6* (8), 5971−5976.

(33) Tanaka, H. Viscoelastic Phase Separation. *J. Phys.: Condens. Matter* **2000**, *12* (15), R207−R264.

(34) Pericet-Camara, R.; Bonaccurso, E.; Graf, K. Microstructuring of Polystyrene Surfaces with Nonsolvent Sessile Droplets. *ChemPhysChem* **2008**, *9* (12), 1738−1746.

(35) Bolognesi, A.; Mercogliano, C.; Yunus, S.; Civardi, M.; Comoretto, D.; Turturro, A. Self-Organization of Polystyrenes into Ordered Microstructured Films and their Replication by Soft Lithography. *Langmuir* **2005**, *21* (8), 3480−3485.

(36) Bassou, N.; Rharbi, Y. Role of Benard-Marangoni Instabilities During Solvent Evaporation in Polymer Surface Corrugations. *Langmuir* **2009**, *25* (1), 624−632.

(37) de Gennes, P. Instabilities During the Evaporation of a Film: Non-Glassy Polymer Plus Volatile Solvent. *Eur. Phys. J. E: Soft Matter Biol. Phys.* **2001**, *6* (5), 421−424.

(38) Sakurai, S.; Furukawa, C.; Okutsu, A.; Miyoshi, A.; Nomura, S. Control of Mesh Pattern of Surface Corrugation via Rate of Solvent Evaporation in Solution Casting of Polymer Film in the Presence of Convection. *Polymer* **2002**, *43* (11), 3359−3364.

(39) de Gennes, P. Solvent Evaporation of Spin Cast Films: "Crust" Effects. *Eur. Phys. J. E: Soft Matter Biol. Phys.* **2002**, *7* (1), 31−34.

(40) Minarik, A.; Perutka, M.; Urban, P.; Lapcik, L.; Juricka, M. A Special Instrument For Exact Control of Self-Organized Structures Preparation in Polymer Layers. *Int. J. Heat Mass Transfer* **2010**, *53* (23−24), 5472−5477.

DOI: 10.1021/acsami.6b15774
ACS Appl. Mater. Interfaces 2017, 9, 6472−6481

(41) Minarik, A.; Smolka, P.; Lapcik, L. Preliminary Investigation of Factors Determining Self-Organised Structures Preparation in Polymer Layers. *Int. J. Heat Mass Transfer* **2011**, *54* (17−18), 4135−4142.
(42) Minarik, A.; Rafajova, M.; Rajnohova, E.; Smolka, P.; Mracek, A. Self-Organised Patterns in Polymeric Films Solidified from Diluted Solutions - The Effect of the Substrate Surface Properties. *Int. J. Heat Mass Transfer* **2014**, *78*, 615−623.
(43) Matsuzaka, K.; Walboomers, X.; Yoshinari, M.; Inoue, T.; Jansen, J. The Attachment and Growth Behavior of Osteoblast-Like Cells on Microtextured Surfaces. *Biomaterials* **2003**, *24* (16), 2711−2719.
(44) Martinez, E.; Engel, E.; Planell, J.; Samitier, J. Effects of Artificial Micro- and Nano-Structured Surfaces on Cell Behaviour. *Ann. Anat.* **2009**, *191* (1), 126−135.
(45) Lucchetta, G.; Sorgato, M.; Zanchetta, E.; Brusatin, G.; Guidi, E.; Di Liddo, R.; Conconi, M. Effect of Injection Molded Micro-Structured Polystyrene Surfaces on Proliferation of MC3T3-E1 Cells. *eXPRESS Polym. Lett.* **2015**, *9* (4), 354−361.
(46) Strawhecker, K.; Kumar, S.; Douglas, J.; Karim, A. The Critical Role of Solvent Evaporation on the Roughness of Spin-Cast Polymer Films. *Macromolecules* **2001**, *34* (14), 4669−4672.
(47) Li, J.; Peng, J.; Huang, W.; Wu, Y.; Fu, J.; Cong, Y.; Xue, L.; Han, Y. Ordered Honeycomb-Structured Gold Nanoparticle Films with Changeable Pore Morphology: From Circle to Ellipse. *Langmuir* **2005**, *21* (5), 2017−2021.
(48) Ruiz-Rubio, L.; Azpitarte, I.; Garcia-Huete, N.; Laza, J.; Vilas, J.; Leon, L. Solvent and Relative Humidity Effect on Highly Ordered Polystyrene Honeycomb Patterns Analyzed by Voronoi Tesselation. *J. Appl. Polym. Sci.* **2016**, *133* (39), 1 DOI: 10.1002/app.44004.
(49) Fragal, V.; Cellet, T.; Fragal, E.; Pereira, G.; Garcia, F.; Nakamura, C.; Asefa, T.; Rubira, A.; Silva, R. Controlling Cell Growth with Tailorable 2D Nanoholes Arrays. *J. Colloid Interface Sci.* **2016**, *466*, 150−161.
(50) Bormashenko, E.; Balter, S.; Pogreb, R.; Bormashenko, Y.; Gendelman, O.; Aurbach, D. On the Mechanism of Patterning in Rapidly Evaporated Polymer Solutions: Is Temperature-Gradient-Driven Marangoni Instability Responsible for the Large-Scale Patterning? *J. Colloid Interface Sci.* **2010**, *343* (2), 602−607.
(51) Lu, M.; Zhang, Y. Microbead Patterning on Porous Films with Ordered Arrays of Pores. *Adv. Mater.* **2006**, *18* (23), 3094−3098.
(52) Chvatalova, L.; Cermak, R.; Mracek, A.; Grulich, O.; Vesel, A.; Ponizil, P.; Minarik, A.; Cvelbar, U.; Benicek, L.; Sajdl, P. The Effect of Plasma Treatment on Structure and Properties of Poly(1-Butene) Surface. *Eur. Polym. J.* **2012**, *48* (4), 866−874.
(53) Junkar, I.; Cvelbar, U.; Vesel, A.; Hauptman, N.; Mozetic, M. The Role of Crystallinity on Polymer Interaction with Oxygen Plasma. *Plasma Processes Polym.* **2009**, *6* (10), 667−675.
(54) Larrieu, J.; Held, B.; Martinez, H.; Tison, Y. Ageing of Atactic and Isotactic Polystyrene Thin Films Treated by Oxygen DC Pulsed Plasma. *Surf. Coat. Technol.* **2005**, *200* (7), 2310−2316.
(55) Kim, B.; Kim, K.; Park, C.; Ryu, C. Improvement of Wettability and Reduction of Aging Effect by Plasma Treatment of Low-Density Polyethylene with Argon and Oxygen Mixtures. *J. Adhes. Sci. Technol.* **2002**, *16* (5), 509−521.
(56) Banik, I.; Kim, K.; Yun, Y.; Kim, D.; Ryu, C.; Park, C. Inhibition of Aging in Plasma-Treated High-Density Polyethylene. *J. Adhes. Sci. Technol.* **2002**, *16* (9), 1155−1169.

DOI: 10.1021/acsami.6b15774
ACS Appl. Mater. Interfaces 2017, 9, 6472−6481